Extra Binding Region Induced by Non-Zinc Chelating Inhibitors into the S_1' Subsite of Matrix Metalloproteinase 8 (MMP-8)†

Giorgio Pochetti,*,‡ Roberta Montanari,‡ Christian Gege,*,§,▽ Carine Chevrier,§ Arthur G. Taveras,||,# and Fernando Mazza‡,⊥

Istituto di Cristallografia—CNR, Area della Ricerca Roma 1, Via Salaria Km.29, 300, I-00016 Monterotondo Stazione, Roma, Italy, Alantos Pharmaceuticals AG, Im Neuenheimer Feld 584, D-69120 Heidelberg, Germany, Alantos Pharmaceuticals Inc., Riverside Technology Center, 840 Memorial Drive, Cambridge Massachusetts 02139, Dipartimento di Scienze della Salute, Università di L'Aquila, I-67010, L'Aquila, Italia

Received September 17, 2008

The mode of binding and the activity of the first two non-zinc chelating, potent, and selective inhibitors of human neutrophil collagenase are reported. The crystal structures of the catalytic domain of MMP-8, respectively complexed with each inhibitor, reveals that both ligands are deeply inserted into the primary specificity subsite S_1', where they induce a similar conformational change of the surrounding loop that is endowed with the main specificity determinants of MMPs. Accord to this rearrangement, both inhibitors remove the floor of the pocket formed by the Y227 side-chain, rendering available an extra binding region never explored before. The present data show that potent and more selective inhibitors can be obtained by developing ligands able to interact with the selectivity regions of the enzyme rather than with the catalytic zinc ion, which is the common feature of all MMP members.

Introduction

Matrix metalloproteinases (MMPs[a]) belong to a family of zinc-endopeptidases that use the electrophilic zinc ion to cleave the constituents of the extracellular matrix.[1] These enzymes are involved in many physiological processes such as ovulation, embryogenesis, angiogenesis, cellular differentiation, and wound healing.[2,3]

Under normal physiological conditions, endogenous tissue inhibitors of MMPs (TIMPs) control their activity.[4] Overexpression of MMP activity, or inadequate control by TIMPs, have been observed and associated with a variety of pathological conditions such as psoriasis,[5] multiple sclerosis,[6,7] osteoarthritis,[8] rheumatoid arthritis,[9,10] osteoporosis,[11,12] Alzheimer's disease,[13] tumor growth and metastasis,[4,14,15] and unwanted degradation of extracellular proteins.

The development of low molecular weight synthetic inhibitors of MMPs is one approach to the therapeutic treatment of these pathologies.[16−18] Many inhibitors have been synthesized and their mode of binding, in the active site of MMPs, have been determined by X-ray crystallography and NMR spectroscopy.[17,19,20] These inhibitors generally include a zinc binding group (ZBG), capable to efficiently chelate the catalytic zinc ion, bound to a substrate-like fragment designed to fit the S_1' primary specificity subsite and adjacent subsites.[21]

Hydroxamate is considered the most effective ZBG because it forms five-membered chelates and two additional H-bonds with the enzyme.[22−24] Hydroxamates, however are affected by lack of selectivity,[25] not only toward the other members of the same family but even to other physiologically important metalloenzymes. Moreover, they show poor pharmacokinetic properties[26] and may cause toxicity resulting from metabolic activation of hydroxylamine.[27] Even though alternative ZBGs have been investigated,[28−34] no MMP inhibitor has emerged on the market, with the sole exception of doxycycline (Periostat), an antibiotic which nonselectively inhibits MMPs.[35]

To overcome the nonselective toxicity, novel MMP inhibitors, which do not bind the catalytic inc ion, have been designed.[36,37] Chen et al.[38] have reported micromolar inhibitors of MMP-13, occupying the S_1' subsite without interacting with the catalytic zinc ion. Engel et al.[39] optimized, on the structural basis, highly selective pyrimidine dicarboxamide inhibitors of MMP-13 characterized by the absence of interactions with the catalytic zinc ion. Morales et al.[40] published the crystal structures of two nonzinc chelating selective inhibitors, respectively complexed with the catalytic domain of MMP-12. Very recently, Johnson et al.[41] and Li et al.[42] showed that a MMP-13 selective inhibitor is absent of musculoskeletal syndrome toxicity and reduces cartilage damage in vivo. Some of these inhibitors are located halfway down the S_1' subsite but the most potent ones[39,41,42] extend deeply into the pocket without removing the floor formed by the F252 side-chain (corresponding to Y227 in MMP-8).

At present, no selective inhibitors of MMP-8 have been discovered. MMP-8 is the most effective collagenase for type 1 collagen and the most active on neutrophils, suggesting a central role in the infiltration of neutrophils. Although MMP-8 is considered as an antitarget for the treatment of cancer,[43] potential indications for the use of selective MMP-8 inhibitors could be in the field of acute liver failure, where MMP-8 deficient mice are resistant to TNF-α induced lethal hepatitis[44] or multiple sclerosis,[45] and other areas including inflammation or cancer progression.[46] The use of such inhibitors could help

† The refined atomic coordinates and processed structure factors amplitudes have been deposited in the Brookhaven Protein Data Bank (PDB) with the following codes: 3DNG, MMP-8:(*S*)-**2**; 3DPE, MMP-8:**1** (monoclinic form); 3DPF, MMP-8:**1** (orthorhombic form).

* To whom correspondence should be addressed. For G.P.: phone, 0039.06.90672627; fax, 0039.06.90672630; E-mail: giorgio.pochetti@ic.cnr.it. For C.G.: phone, 0049.6221.7390181; fax, 0049.6221.7390139; E-mail, christian.gege@web.de.

‡ Istituto di Cristallografia—CNR.

§ Alantos Pharmaceuticals AG.

|| Alantos Pharmaceuticals Inc.

⊥ Dipartimento di Scienze della Salute, Università di L'Aquila.

Present address: Biogen Idec Inc., 14 Cambridge Center, Cambridge Massachusetts 02142.

▽ Present address: X2-Pharma GmbH, Im Neuenheimer Feld 584, D-69120 Heidelberg, Germany.

[a] Abbreviations: MMP, matrix metalloproteinase; TIMP, tissue inhibitor of MMP; ZBG, zinc binding group; AH, acetohydroxamate; EDCI, 1-(3-dimethylaminopropyl)-3-ethylcarbodiimide hydrochloride; HOAt, 1-hydroxy-7-azabenzotriazole; NMM, *N*-methylmorpholine.

10.1021/jm801166j CCC: $40.75
Published on Web 01/27/2009

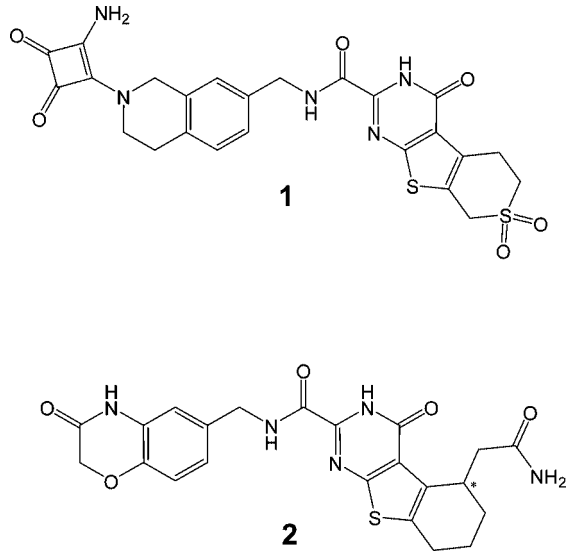

Figure 1. Chemical structure of **1** and **2**.

to determine the relevance of the MMP-8 enzyme as a novel therapeutic target for these diseases.

Here we report the activity and mode of binding of the first two nonzinc chelating inhibitors of human neutrophil collagenase.[47] Both ligands inhibit MP-8 with activity in the low nM range and are highly selective versus several other MMPs. The crystal structures of the complexes show that both ligands deeply insert into the primary specificity pocket S_1' induce a dramatic conformational change of the loop delimiting the pocket, removing the floor formed by the aromatic side-chain of Y227, and disclose an extra binding region never explored in other MMP-8 complexes. Their high selectivity profile can be attributed to the conformational change induced to the S_1' loop, which is known to present a considerable variation in the size, shape and composition among the MMPs.

Results and Discussion

Chemistry. Compounds **1** and **2** (Figure 1) were prepared according to the synthetic sequence outlined in Scheme 1. Thus, cyclization of commercially available ethyl 2-amino-4,7-dihydro-5*H*-thieno[2,3-*c*]thiopyran-3-carboxylate 6,6-dioxide **3** with ethyl cyanoformate in hydrochloric acid afforded ester **4**, which was deprotected with excess of aqueous lithium hydroxide to give acid **5**, which was finally coupled with amine **6**[50] using 1-(3-dimethylaminopropyl)-3-ethylcarbodiimide hydrochloride (EDCI), 1-hydroxy-7-azabenzotriazole (HOAt) and *N*-methylmorpholine (NMM) to yield **1** after aqueous workup. Knoevenagel condensation of (2-oxo-cyclohexyl)-acetic acid ethyl ester **7** with ethylcyanoacetate afforded intermediate **8**, which was transformed via Gewald reaction with sulfur to the thiophene derivative **9**. Cyclization as described above furnished ester **10**, which was selectively saponified with 2 equiv of aqueous lithium hydroxide to afford the monoacid **11**. Coupling with 6-aminomethyl-4*H*-benzo[1,4]oxazin-3-one building block **12**[50] furnished derivative **13**, which was saponified to acid **14** and finally coupled with ammonium chloride using EDCI, HOAt, and NMM to afford inhibitor **2** as racemate.

Zinc Coordination. The enzyme essential catalytic machinery is formed by the Zn ion, coordinated by the three H residues belonging to the binding motif HEXXHXXGXXH, and the water molecule bridged with the glutamate of the same motif.

A comparison of the active site of our complexes with that of the uninhibited enzyme[48] shows that the Zn coordination is

Scheme 1. Synthesis of Compounds **1** and **2**[a]

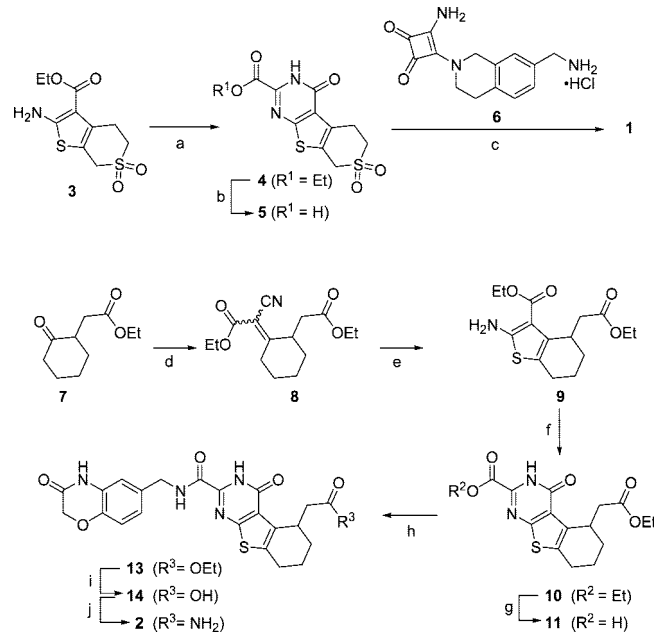

[a] Reagents and conditions: (a) $CNCO_2Et$, 4 N HCl·dioxane, 50 °C; (b) 1 N LiOH; (c) **6**, EDCI, HOAt, NMM, DMF; (d) $CNCH_2COOEt$, AcOH, NH_4OAc, reflux; (e) sulphur, $HNEt_2$, MeOH, 50 °C; (f) $CNCO_2Et$, 4 N HCl·dioxane, 50 °C; (g) 1 N LiOH (2 equiv); (h) **12**, EDCI, HOAt, NMM, DMF; (i) 1 N LiOH; (j) NH_4Cl, EDCI, HOAt, NMM, DMF.

unchanged. In all cases, we have observed a distorted tetrahedral coordination, with the largest angle involving the water and H207. The zinc ion does not interact with the inhibitors, the shortest distances between the Zn ion and the inhibitor atoms being 4.5 Å (Figure 2).

Moreover, the electron density found for the water oxygen in the various complexes is of spherical or elipsoidal shape. This observation can be related to the catalytic role played by the water, requiring its possible mobility. In fact, the water should be activated by the catalytic glutamate prior the nucleophilic attack to the substrate scissile peptide bond.

Inhibitor Mode of Binding. The chemical formulas of the inhibitors are shown in Figure 1. Their central scaffold, formed by two fused-ring systems separated by a methylencarboxamide group, presents similar size and shape. Main differences are given by the squaramide moiety bound to one terminal end of **1** and by the carbamoylmethyl substituent, attached to the asymmetric carbon atom at the opposite end of **2**.

Two crystal forms, one monoclinic and the other orthorhombic, respectively containing one and two enzyme−inhibitor complexes per asymmetric unit, have been found when we cocrystallized MMP-8 with **1** (MMP-8:**1** complex). A monoclinic form, containing two complexes per asymmetric unit, was obtained for the *S* enantiomer of **2** (MMP-8:(*S*)-**2** complex). The cocrystallization trials for obtaining the MMP-8:(*S*)-**2** complex were performed by adding the racemic mixture of **2** to the enzyme. In the first attempt to fit the ligand in the Fourier difference map, electron density was clearly evident for the carbamoylmethyl group as substituent of the asymmetric carbon with *S* configuration.

The mode of binding of each inhibitor in the independent units is similar, and the central scaffold of the two inhibitors gives rise to similar interactions with the enzyme in all complexes.

Both inhibitors are deeply inserted into the primary specificity pocket S_1', where they adopt an extended conformation with

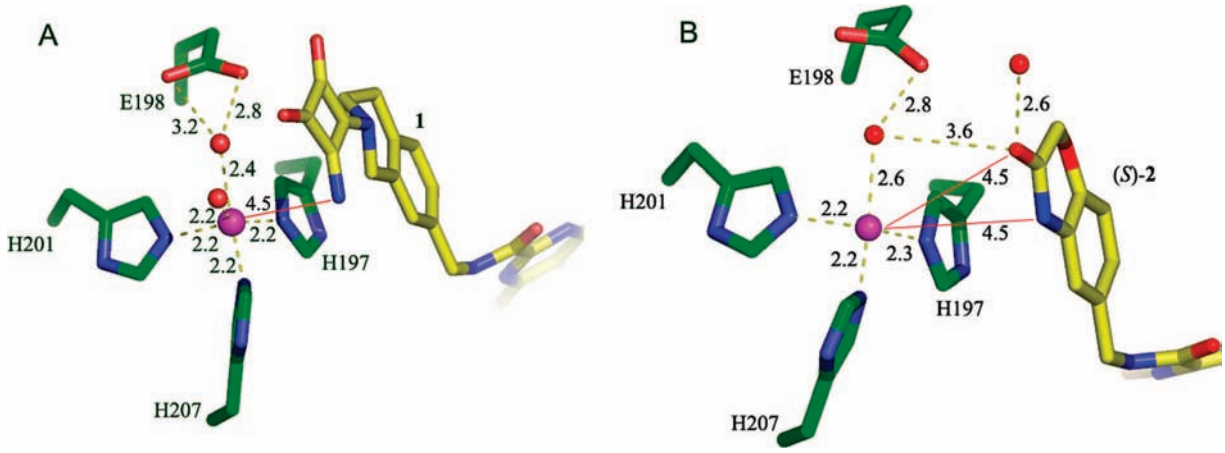

Figure 2. Zinc coordination: (A) in the complex MMP-8:**1**, and (B) in the complex MMP-8:(*S*)-**2**.

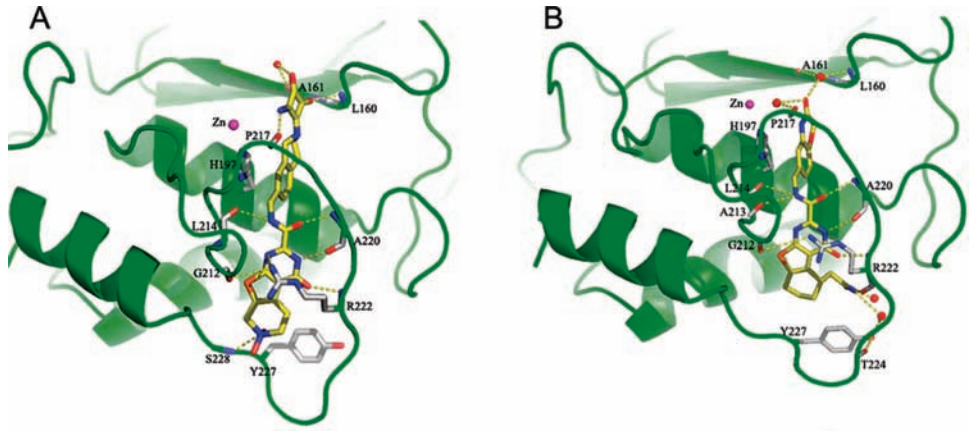

Figure 3. H-bonds (dashed lines) formed by (A) **1** and (B) (*S*)-**2** in the active site of MMP-8.

the mean planes of the two fused-ring systems almost perpendicular to each other. The binding modes found in MMP-8:**1** and MMP-8:(*S*)-**2** crystals are reported in parts A and B of Figure 3, respectively, and their similar interactions are the following. The aromatic cloud of the H197 imidazole ring gives rise to a π-stacking interaction, respectively with that of the isoquinoline of **1** and the benzoxazinone of (*S*)-**2**. The NH and CO of the central carboxamide group of both inhibitors form H-bonds with the L214CO and A220NH, respectively. The NH and CO groups of the 3*H*-pyridin-4-one ring of both ligands engage H-bonds with the A220CO and R222NH groups, respectively. The charged guanidinium group of R222 stacks onto the aromatic cloud of the 3*H*-thieno[2,3-*d*]pyrimidin-4-one system of both inhibitors, giving rise to cation$-\pi$ interactions. The extended conformation of the R222 side-chain is also favored by the H-bond between its guanidinium group and the G212CO belonging to the facing loop.

The different binding interactions involving the terminal parts of the two inhibitors are as follows. The NH groups of L160 and A161 residues, both belonging to the antiparallel β-strand forming the upper rim of the active site, give rise to a bifurcated H-bond with one carbonyl of the squaramide ring of **1**, whereas they engage at the same way the carbonyl of the benzoxazinone ring of (*S*)-**2** through a bridged water molecule. It is worth noting that the substrate-enzyme H-bond with L160NH is always conserved in the crystal complexes of MMP-8 available on PDB. The CO group of P217, a residue located at the entrance of the S_1' pocket, is H-bond acceptor from the amino group of the squaramide ring of **1**, and from the NH of the benzoxazinone ring of (*S*)-**2**. The NH of S228, a residue at the end of the S_1' loop, engages both sulfonyl oxygens of **1** through a bifurcated H-bond. The terminal carbamoyl group of (*S*)-**2**, pointing toward the central part of the S_1' loop, forms a complex H-bonding network involving R222CO and Y227OH. The inhibitor NH_2 is H-bond donor to the R222CO. The Y227OH is H-bond donor to the T224CO and acceptor of a bifurcated H-bond from both the NH and CO groups of the inhibitor carbamoyl moiety; each branch of the bifurcated H-bond is bridged by one water molecule. The similar relative position of the central scaffold of the two inhibitors can be appreciated by the superposition of their crystal complexes shown in Figure 4.

Inhibitor Induced Conformational Changes at the S_1' loop. A comparison between the crystal form of the uninhibited MMP-8 and the inhibitor-bound complexes reported here reveals important structural differences regarding essentially the S_1' specificity loop. The first part of this loop, containing the third Zn-coordinated H207 and two consecutive β-turns (210−216) with the strictly invariant M215, remains practically unaltered. Large conformational changes are induced by both inhibitors on the segment 219−229, separating the tube-like crevice from bulk water. The largest C^{α} displacements induced by both inhibitors occur for the sequence R222−N226, as reported in Table S1 (Supporting Information). As a consequence, the Y227 side-chain of both complexes has been pushed from the position occupied in the uninhibited enzyme. At this regard, we have examined the position of Y227 in the crystals of all the other inhibited MMP-8, available on the PDB. In all cases, this residue practically occupies the same position as that of the uninhibited MMP-8, forming the floor of the S_1' pocket, and the S_1' loop maintains essentially the same conformation (Figure 5). It should

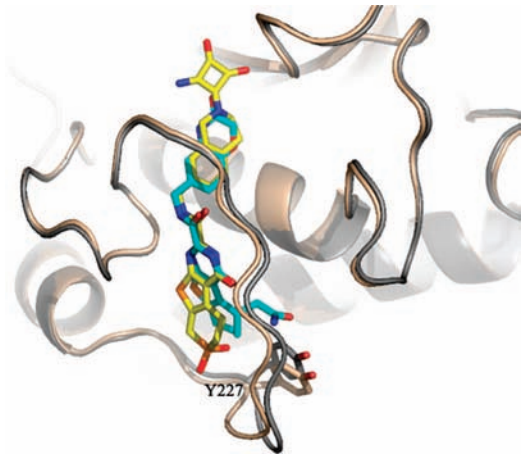

Figure 4. Superposition between MMP-8:**1** (inhibitor in yellow color) and MMP-8:(*S*)-**2** (inhibitor in cyan color). The protein trace (gray color for MMP-8:**1**) of both complexes is shown.

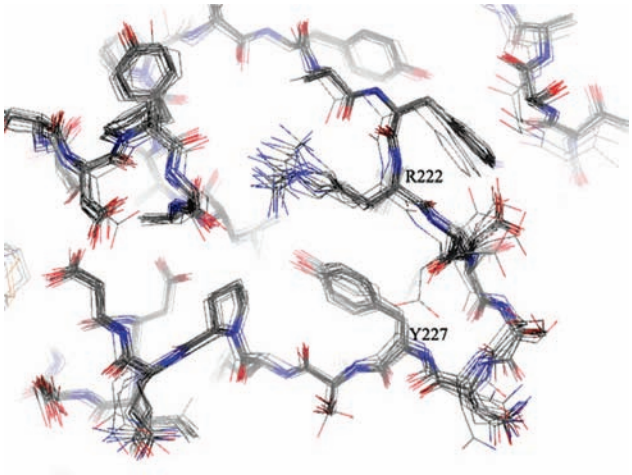

Figure 5. Side view of the S_1' specificity loop obtained by superposition of the uninhibited MMP-8 (PDB code 2OY4) and 17 inhibited complexes of MMP-8 available on PDB (PDB codes: 1JAN, 1JAP, 1I73, 1I76, 1ZVX, 1ZS0, 1MNC, 1MMB, 1JJ9, 1JAQ, 1JAO, 1A86, 1KBC, 1BZS, 1JH1, 1ZP5, 2OY2).

be noted that none of the previous known inhibitors was long enough to approach the side-chain of Y227. Figure 6A represents a superposition between the MMP-8 complexed with a phosphonate inhibitor (PDB accession code 1ZVX) representing the deepest P_1' group (cyan color), as known before the present finding, and the MMP-8:(*S*)-**2** complex (yellow color). The comparison with MMP-8:**1** is very similar, and it has been omitted from Figure 6A for clarity. There, it can be noted that the conformational change of Y227 side-chain is determined by the tricyclic ring system in order to avoid steric overlapping between their rings. The switching of the Y227 side-chain is realized with a concerted rearrangement of the S_1' loop involving the region R222−Y227. In this way, an extra-binding region at the bottom of the primary specificity subsite S_1' is rendered accessible, as shown in Figure 6B. There, the van der Waals surface of (*S*)-**2** (blue color) and that of the phosphonate inhibitor mentioned above are reported (yellow color). The new position of Y227 side-chain shows that the extra-binding region becomes available whenever the switching of this side-chain occurs. Therefore, the Y227 residue plays the role of "selective gatekeeper", rendering accessible the extra binding region of the S_1' specificity subsite.

Conformational changes of such extent have never been observed in the previous inhibited crystal complexes of MMP-8 available on the PDB. Our ligands constitute the first example of the most profound occupation of the MMP-8 S_1' specificity pocket.

The inhibitors disclosed here show activities in the nanomolar range against MMP-8, as reported in Table 1, although their binding is limited to the S_1' hydrophobic pocket, without interacting with the catalytic zinc ion.

The 8× potency difference between **1** and **2** could be of 16× considering that the IC_{50} reported for **2** represents that of the racemic mixture. This difference can be rationalized as follows. As shown in Figure 4, both inhibitors induce a similar conformational change of the specificity loop, with the rearrangement of the Y227 side-chain toward a "floor-out" conformation, but, at variance with **1**, the carbamoyl group of **2** protrudes even further toward the extra binding region. There, the *S* enantiomer stabilizes better than **1** the opening to the extra binding region through the H-bonding network with Y227OH, as previously described. The new conformation of the specificity loop is further on stabilized by a H-bond between the Y227OH and the T224CO (see Figure 3B and Figure 7).

Selectivity against Other MMPs. The selectivity profile of our inhibitors can be deduced from inspection of Table 1, where their activities against other MMPs are reported. To investigate the role of the S_1' specificity loop for MMP-8 selectivity, we aligned the amino acid sequence of this loop with that of other MMP members of known 3D structure, as reported in Table 2.

Conformational restrictions appear obvious for those specificity loops shorter than that of MMP-8. In particular, MMP-1, MMP-2, and MMP-9 present two consecutive deletions in correspondence of positions 224 and 225 of MMP-8, where the largest C^{α} displacements occur in the reported complexes. For MMP-7, although there is one deletion only for the above-mentioned position 225, the conformationally restricted Pro, occurring just two residues before that deletion, causes a kink and consequently a shrinking of the S_1' loop.

Conformational restrictions for MMPs with similar or longer loops should be based on the equivalent positions, which may not be able to adopt the complementary geometry required to form favorable interactions between the specificity loop and the inhibitors.

Comparison among MMP-8, MMP-13, and MMP-3. The ligands here described are also active against MMP-13, for which selective inhibitors, deeply inserted into the S_1' pocket and not interacting with the zinc ion, have been described.[39,41] In this regard, we have checked the putative occupation of our inhibitors into the S_1' subsite of MMP-13. We deduced that it could take place if the F252, equivalent to the Y227 in MMP-8, and the loop region 247−252 would adopt a conformational change analogous to that found in our MMP-8 complexes.

Parts A and B of Figure 8 show a C^{α} superposition of MMP-8:**1**, MMP-8:(*S*)-**2** and MMP-13 bound to nonzinc chelating inhibitors (PDB codes 1XUR and 2OW9). While the central scaffold of the MMP-13 inhibitors leaves unperturbed the "floor-in" conformation of F252, the bulkier tricylic ring system of MMP-8 inhibitors causes the switching of Y227 toward the "floor-out" conformation. Moreover, a cation−π interaction is realized by the aromatic scaffold of **1** and (*S*)-**2** with the R222 of MMP-8. It should be noted that in the sequence alignment among MMPs reported in Table 2, R222 is the only positively charged residue in this position. The shorter and uncharged side-chain of T226 in MMP-13, equivalent to R222 in MMP-8, is unable to give the same interaction. The lack of the cation−π

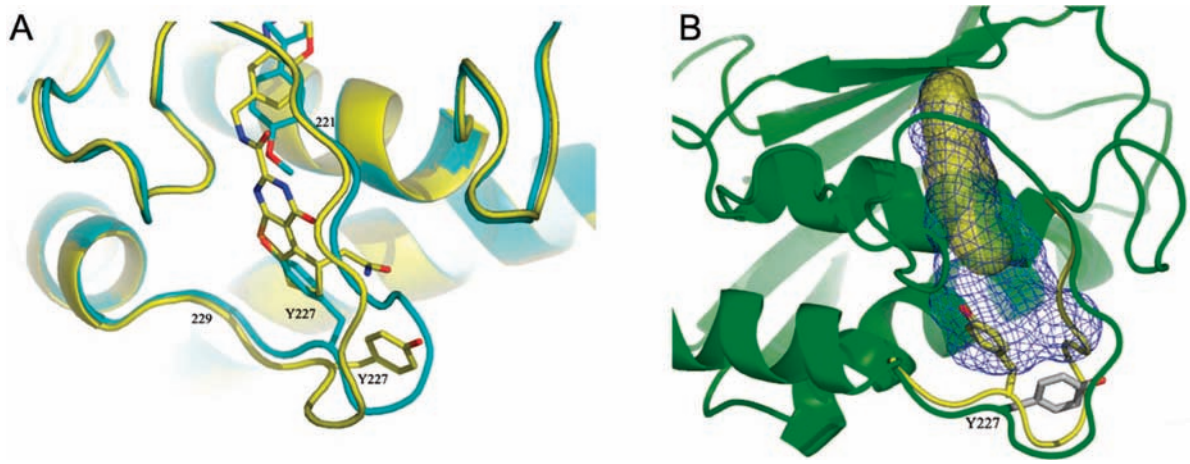

Figure 6. (A) superimposed crystal structures of MMP-8 complexed, respectively with the phosphonate inhibitor (PDB code 1ZVX, cyan color) and the compound (*S*)-**2** (yellow color); (B) extra binding region deducible as difference between the van der Waals surfaces of the inhibitors shown in (A). The vdW surface is blue colored around (*S*)-**2** and yellow colored around the phosphonate inhibitor. The Y227 side-chain in the two complexes is also presented.

Table 1. IC_{50} Values (nM) of **1** and **2** against MMPs[a]

	MMP-1	MMP-2	MMP-3	MMP-7	**MMP-8**	MMP-9	MMP-12	MMP-13	MMP-14
1	>10000	>2500	<100	>10000	**57**	>10000	>5000	<25	>10000
2	>10000	>10000	>2500	>10000	**7.4**	>10000	>10000	<25	>10000

[a] Errors are in the range of 5−10% of the reported value. IC_{50} values of **2** have been determined for the racemic mixture.

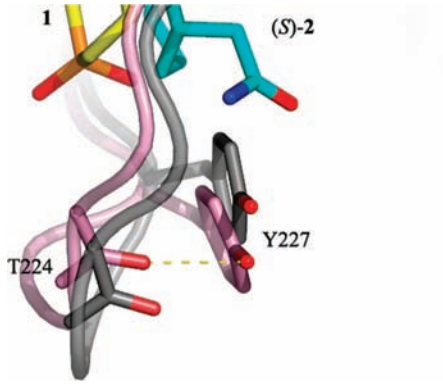

Figure 7. Details of the MMP-8 specificity loop: C^{α} superposition of the complexes of MMP-8 (gray) with **1** (yellow color) and (*S*)-**2** (cyan color). MMP-8 trace is shown in magenta for the complex with (*S*)-**2**.

Table 2. Structure-Based Sequence Alignment of Known Crystal Structure MMPs[a]

	219	220	—	221	222	223	224	225	226	227	228	229
MMP-8	Y	A	—	F	R	E	T	S	N	Y	S	L
MMP-1	Y	T	—	F	S	G	—	—	D	V	Q	L
MMP-2	Y	T	—	Y	T	K	—	—	N	F	R	L
MMP-3	Y	H	S	L	T	D	L	T	R	F	R	L
MMP-7	Y	G	N	G	D	P	Q	—	N	F	K	L
MMP-9	Y	R	—	F	T	E	—	—	G	P	P	L
MMP-12	Y	K	—	Y	V	D	I	N	T	F	R	L
MMP-13	Y	T	—	Y	T	G	K	S	H	F	M	L
MMP-14	Y	Q	—	W	M	D	T	E	N	F	V	L

[a] The region shown corresponds to the S_1' loop and the numbering refers to the MMP-8.

interaction could be compensated by the presence of the charged residue K228 of MMP-13 (T224 in MMP-8) capable to give electrostatic interactions, as observed in the structures of the complexes of MMP-13 with selective inihibitors (PDB accession codes 2OW9 and 2OZR).

Our inhibitors show a reduced activity toward MMP-3, whose S_1' loop is one residue longer than that of MMP-8. The inspection of the inhibited complexes available on PDB shows that the S_1' loop of MMP-3 can adopt two different arrangements. In one case, an additional β-turn (PDB code: 2D1O), or a γ-turn (PDB code: 1B32) can be formed in the region 224−227. These secondary structure elements lack in the equivalent region (220−222) of MMP-8, where A220 and R222 form three key H-bonds with our inhibitors, as shown in the superposition given in Figure 9A. In the other case (PDB code: 1CAQ, 1CIZ), the region 224−227 of MMP-3 has a conformation similar to that equivalent of MMP-8 and therefore capable to form the key H-bonds with our ligands. However, the additional β-turn is shifted forward at the region 228−231, equivalent to that 224−227 of MMP-8, where the largest C^{α} displacements have been induced by our inhibitors (see Figure 9B). This β-turn and the additional residue at this position could preclude the optimal geometry of the loop required to give complementary interactions with (*S*)-**2**, particularly, the complex H-bonding network formed by the carbamoyl group of (*S*)-**2**, which points toward the central part of S_1' loop (see Figure 3B). This could explain the activity of **2** significantly lower than **1** against MMP-3.

In conclusion, the longer S_1' loop of MMP-3, rather than increase its internal flexibility, gives rise to a structural organization that can hinder the optimal geometry required by productive enzyme−ligand interactions.

Conclusions

Inhibitors without the ZBG typically risk losing potency while gaining selectivity. In fact, zinc binding, the common feature of all MMP members, follows a rather universal recognition motif. Although lacking the ZBG, the inhibitors disclosed here show activity against MMP-8 in the nanomolar range. Moreover, their high selectivity profile can be attributed to the conformational change induced to the S_1' loop. In fact, it is known that this loop presents a considerable variation in the composition, size, and shape among the MMP family members. Therefore, the present data show that potent and more selective inhibitors

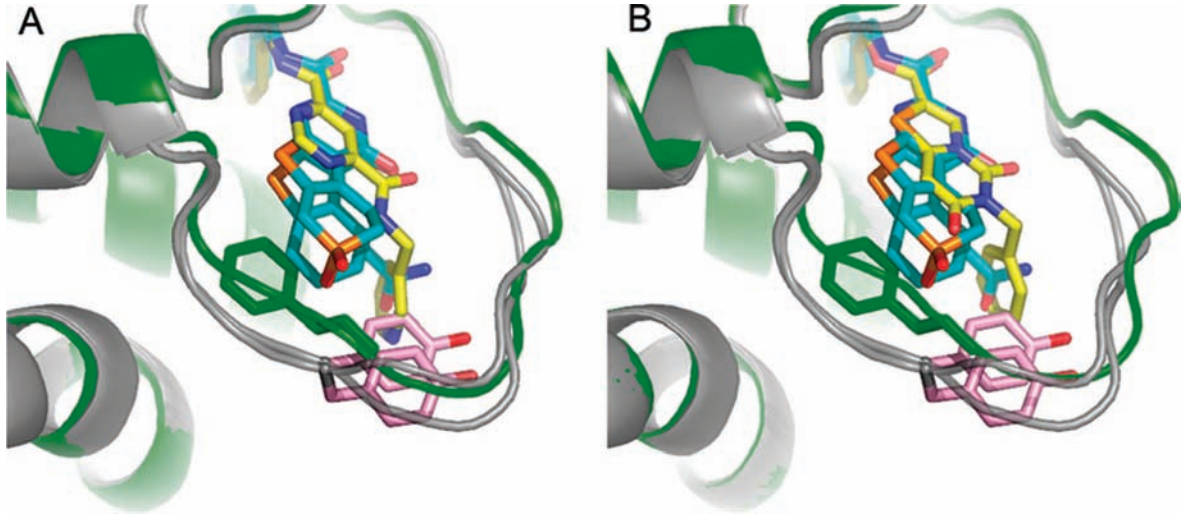

Figure 8. Comparison of MMP-8/MMP-13 complex structures: C^{α} superposition of the complexes of MMP-8 (gray) with **1** and (*S*)-**2** (cyan) and MMP-13 (green) with (A) a pyrimidine dicarboxamide inhibitor (yellow) (PDB code: 1XUR), and (B) a selective inhibitor (yellow) (PDB code: 2OW9). In both figures, Y227 of MMP-8 is shown in pink, the equivalent F252 of MMP-13 in green.

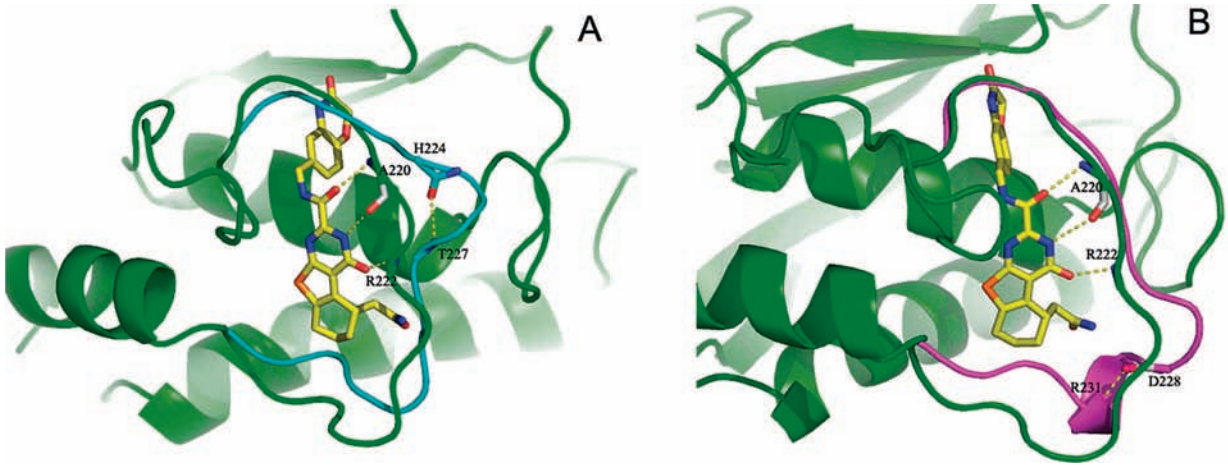

Figure 9. Comparison of MMP-8/MMP-3 complex structures: side view of the S_1' specificity loop obtained by superposition of MMP-8:(*S*)-**2** (protein trace in green color, (*S*)-**2** in yellow) and (A) MMP-3 (PDB code 2D1O, cyan color), (B) MMP-3 (PDB code 1CAQ, purple color).

can be obtained by targeting selective regions of the enzyme, rather than the catalytic zinc ion. In this way, the inhibitor can select the appropriate complementary sequence from the conformational ensemble of the apo enzyme.

In light of the present data, it could be argued that inhibitor binding of MMP-8 is not a simple diffusion process. On the contrary, inhibition takes place through an induced fit mechanism operating on the loop surrounding the S_1' subsite, which defines the shape and the size of the pocket.[49]

This induced fit mechanism operating on the S_1' loop opens an extra binding region of the pocket by the switching of the Y227 side-chain, which plays the role of a selective gatekeeper. This extra binding region has never been explored in the previously examined complexes of MMP-8 reported on the PDB. Moreover, C^{α} displacements of the S_1' loop residues as large as those reported have never been evidenced in any MMP-8 complex with known inhibitors and the removal of the floor of the S_1' pocket has never been observed in any MMP-complex. Further molecular modeling studies, aimed to increase ligand−enzyme interactions, could consider the displacement of the two water molecules, bridged in the bifurcated H-bond between the terminal carbamoyl group of (*S*)-**2** and the hydroxyl of Y227 in order to form a direct H-bond with the Y227 side-chain.

Finally, the sequence alignment of S_1' specificity loop among MMPs shows that MMP-8 differs from the other members for two residues: the unique positively charged R222 and the Y227 forming the floor. A phenylalanine residue, unable to form a H-bond, replaces the tyrosine residue in the other MMP members. The key position in the loop of these two residues offers interesting hints for designing new and more selective inhibitors of MMP-8.

Experimental Section

Chemical Methods. ^{1}H NMR spectra were recorded on a Bruker Avance (250 MHz) instrument at 300 K in $CDCl_3$, or DMSO-d_6. Chemical shifts are reported in δ values (ppm); the hydrogenated residues of deuterated solvent were used as internal standard ($CDCl_3$: δ 7.26 and DMSO: δ 2.50). Signals are described as s, d, t, dd, m, and b for singlet, doublet, triplet, double−doublet, multiplet, and broad, respectively. Mass spectra (LC-MS) were measured on a Ion Trap Esquire 3000+ instrument. Microanalyses of target compounds were carried out with an Eurovector Euro 3000 model analyzer; the analytical results are within ±0.4% of theoretical values. Chemical names follow IUPAC nomenclature. Starting materials were purchased from Aldrich, Acros, Lancaster, Fluka, or Enamine (for compound **3**) and were used without purification. Column chromatography was performed using silica gel (40−63 μm), and the reaction progress was determined by thin

layer chromatography analyses on Merck silica gel plastic plates $60F_{254}$. The following compounds were prepared according to previously described procedures: 3-amino-4-(7-aminomethyl-3,4-dihydro-1*H*-isoquinolin-2-yl)-cyclobut-3-ene-1,2-dione hydrochloride (**6**),[50] and 6-aminomethyl-4*H*-benzo[1,4]oxazin-3-one hydrochloride (**12**).[50]

4,7,7-Trioxo-3,4,5,6,7,8-hexahydro-7,9-dithia-1,3-diaza-fluorene-2-carboxylic Acid Ethyl Ester (4). To a solution of ethyl 2-amino-4,7-dihydro-5*H*-thieno[2,3-*c*]thiopyran-3-carboxylate 6,6-dioxide (500 mg, 1.81 mmol) in hydrochloric acid (4 M in dioxane; 10 mL) was added ethyl cyanoformate (270 μL, 2.72 mmol). The mixture was stirred at 50 °C for 4 h and concentrated under reduced pressure. The residue was dissolved in ethyl acetate, washed with water and then brine, and dried over $MgSO_4$. After evaporation the crude product was obtained as orange solid (524 mg, 88%). ^{1}H NMR (DMSO-d_6): δ 8.06 (d, 1H, NH), 4.71 (s, 2H, CH_2SO_2), 4.36 (q, 2H, CH_2Me), 3.50 (s, 4H, $CH_2CH_2SO_2$), 1.34 (t, 3H, CH_3). $C_{12}H_{12}N_2O_5S_2$; MW: 328; MS 329 $[M + H]^+$.

4,7,7-Trioxo-3,4,5,6,7,8-hexahydro-7,9-dithia-1,3-diaza-fluorene-2-carboxylic Acid (5). To a solution of ester **4** (300 mg, 0.91 mmol) in THF (10 mL) was added 1 M LiOH (2.75 mL, 2.75 mmol). The mixture was stirred at room temperature for 90 min and then the solvent removed by evaporation at 30 °C. The mixture was acidified by addition of 1N HCl and the precipitate filtered and dried under high vacuum to afford the product as a pale-brown solid (85 mg, 31%). ^{1}H NMR (DMSO-d_6): δ 4.66 (s, 2H, CH_2SO_2), 3.42 (bs, 4H, $CH_2CH_2SO_2$). $C_{10}H_8N_2O_5S_2$; MW: 300; MS 301 $[M + H]^+$.

4,7,7-Trioxo-3,4,5,6,7,8-hexahydro-7,9-dithia-1,3-diaza-fluorene-2-carboxylic Acid [2-(2-Amino-3,4-dioxo-cyclobut-1-enyl)-1,2,3,4-tetrahydro-isoquinolin-7-ylmethyl]-amide (1). To a solution of acid **5** (40 mg, 0.13 mmol), EDCI (51 mg, 0.26 mmol), and HOAt (18 mg, 0.13 mmol) in DMF (3 mL) were added NMM (100 μL) and 3-amino-4-(7-aminomethyl-3,4-dihydro-1*H*-isoquinolin-2-yl)-cyclobut-3-ene-1,2-dione hydrochloride **6** (47 mg, 0.16 mmol). The mixture was stirred overnight at room temperature and then concentrated. The remaining residue was suspended in 10% aqueous citric acid and the residue was filtered and dried. After recrystallization in MeOH the desired product was obtained (32 mg, 44%) as an off-white solid. ^{1}H NMR (DMSO-d_6): δ 12.47 (bs, 1H, NH), 9.68 (t, 1H, NH), 7.80 (s, 2H, NH_2), 7.17−7.10 (m, 3H, aromatic), 4.87 (bs, 2H, CH_2SO_2), 4.68 (s, 2H, CH_2N), 4.39 (d, 2H, CH_2NH), 3.93 (bs, 2H, $CH_2CH_2SO_2$), 3.50 (s, 4H, NCH_2CH_2 + C$H_2CH_2SO_2$), 2.93−2.84 (m, 2H, NCH_2CH_2). Anal. ($C_{24}H_{21}N_5O_6S_2$) C, H, N, S. MW: 539; MS 540 $[M + H]^+$.

Cyano-(2-ethoxycarbonylmethyl-cyclohexylidene)-acetic Acid Ethyl Ester (8). A solution of (2-*oxo*-cyclohexyl)-acetic acid ethyl ester (1.00 g, 5.43 mmol), ethyl cyanoacetate (0.80 g, 7.05 mmol), acetic acid (100 μL), and ammonium acetate (40 mg) in toluene was refluxed overnight with a Dean−Stark apparatus. After the solution was cooled to room temperature, the solvent was removed and the residue purified by flash chromatography on silica gel using cyclohexane/ethyl acetate 8/2 as eluent. The crude product (1.5 g) was obtained as a yellow oil and used without further purification in the next step. ^{1}H NMR ($CDCl_3$): δ 4.29−4.24 (m, 2H, CH_2Me), 4.17−4.08 (m, 2H, CH_2Me), 2.88−1.61 (m, 11H, CH, 5 CH_2), 1.37−1.22 (m, 6H, 2 CH_3). $C_{15}H_{21}NO_4$; MW: 279; MS 280 $[M + H]^+$.

2-Amino-4-ethoxycarbonylmethyl-4,5,6,7-tetrahydro-benz[*b*]-thiophene-3-carboxylic Acid Ethyl Ester (9). A solution of compound **8** (980 mg, 3.5 mmol) and sulfur (125 mg, 3.86 mmol) in MeOH was heated at 50 °C and then diethylamine (180 μL, 1.75 mmol) was added slowly. After 4 h at 50 °C, the solvent was removed by evaporation. The residue was purified by flash chromatography using cyclohexane/ethyl acetate 8/2 as eluent to give the thiophene derivative (517 mg) as yellow oil. The presence of starting material was still detectable but the product was used without further purification. ^{1}H NMR ($CDCl_3$): δ 6.08 (s, 2H, NH_2), 4.27 (q, 2H, CH_2Me), 4.14 (q, 2H, CH_2Me), 3.62 (bd, 1H, CH), 2.90−1.62 (m, 8H, 4 CH_2), 1.41−1.22 (m, 6H, 2 CH_3). $C_{15}H_{21}NO_4S$; MW: 311; MS 312 $[M + H]^+$.

5-Ethoxycarbonylmethyl-4-*oxo*-3,4,5,6,7,8-hexahydro-benzo[4,5]thieno[2,3-*d*]pyrimidine-2-carboxylic Acid Ethyl Ester (10). To a solution of compound **9** (515 mg, 1.65 mmol) in hydrochloric acid (4 M in dioxane; 10 mL) was added ethyl cyanoformate (250 μL, 2.48 mmol). The mixture was stirred at 50 °C for 2 h and concentrated under reduced pressure. The residue was dissolved in ethyl acetate, washed with water and then brine, and dried over $MgSO_4$. After evaporation the crude product was purified by flash chromatography using dichloromethane/methanol 98/2 as eluent to afford the desired product as yellow solid (165 mg, 27%). ^{1}H NMR ($CDCl_3$): δ 9.87 (s, 1H, NH), 4.54 (q, 2H, CH_2Me), 4.16 (q, 2H, CH_2Me), 3.86 (bd, 1H, CH), 2.98 (dd, 1H, C*H*HCO), 2.86−2.77 (m, 2H, CH_2), 2.47 (dd, 1H, CH*H*CO), 1.97−1.87 (m, 4H, 2 CH_2), 1.47 (t, 3H, CH_3), 1.27 (t, 3H, CH_3). $C_{17}H_{20}N_2O_5S$; MW: 364; MS 365 $[M + H]^+$.

5-Ethoxycarbonylmethyl-4-*oxo*-3,4,5,6,7,8-hexahydro-benzo[4,5]thieno[2,3-*d*]pyrimidine-2-carboxylic Acid (11). To a solution of ester **10** (160 mg, 0.44 mmol) in THF (10 mL) was added 1 M LiOH (0.88 mL, 0.88 mmol). The mixture was stirred at room temperature for 30 min and acidified by addition of 1N HCl. The precipitate was filtered and dried under high vacuum to afford the product as a white solid (130 mg, 88%). ^{1}H NMR (DMSO-d_6): δ 4.08 (q, 2H, CH_2Me), 3.65 (bd, 1H, CH), 2.85 (dd, 2H, CH_2CO), 2.48−2.35 (m, 2H, CH_2), 1.85−1.75 (m, 4H, 2 CH_2), 1.18 (t, 3H, CH_3). $C_{15}H_{16}N_2O_5S$; MW: 336; MS 337 $[M + H]^+$.

{4-*oxo*-2[(3-*oxo*-3,4-Dihydro-2*H*-benzo[1,4]oxazin-6-ylmethyl)-carbamoyl]-3,4,5,6,7,8-hexahydrobenzo[4,5]thieno[2,3-*d*]pyrimidin-5-yl}-acetic Acid Ethyl Ester (13). To a solution of acid **11** (120 mg, 0.36 mmol), EDCI (137 mg, 0.71 mmol), and HOAt (48 mg, 0.36 mmol) in DMF (3 mL) were added NMM (300 μL) and 6-aminomethyl-4*H*-benzo[1,4]oxazin-3-one hydrochloride **12** (92 mg, 0.43 mmol). The mixture was stirred overnight at room temperature and then concentrated. The remaining residue was suspended in 10% aqueous citric acid, and the residue was filtered and dried to afford the product (175 mg, 99%) as an off-white solid. ^{1}H NMR (DMSO-d_6): δ 12.34 (bs, 1H, NH), 10.68 (s, 1H, NH), 9.63 (t, 1H, NH), 6.89 (m, 3H, aromatic), 4.52 (s, 2H, CH_2O), 4.32 (d, 2H, CH_2N), 4.08 (q, 2H, CH_2Me), 3.65 (bd, 1H, CH), 2.89−2.73 (m, 3H, CH_2 + C*H*H), 2.46−2.35 (m, 1H, CH*H*), 1.88−1.68 (m, 4H, 2 CH_2), 1.18 (t, 3H, CH_3). $C_{24}H_{24}N_4O_6S$; MW: 496; MS 497 $[M + H]^+$.

{4-*oxo*-2[(3-*oxo*-3,4-Dihydro-2*H*-benzo[1,4]oxazin-6-ylmethyl)-carbamoyl]-3,4,5,6,7,8-hexahydrobenzo[4,5]thieno[2,3-*d*]pyrimidin-5-yl}-acetic Acid (14). To a solution of ester **13** (200 mg, 0.40 mmol) in THF (10 mL) was added 1 M LiOH (1.2 mL, 1.2 mmol). The mixture was stirred at room temperature for 4 h and acidified by addition of 1N HCl. The precipitate was filtered and dried under high vacuum to afford the product as a white solid (150 mg, 80%). ^{1}H NMR (DMSO-d_6): δ 12.35 (s, 1H, NH), 10.68 (s, 1H, NH), 9.63 (t, 1H, NH), 6.89 (m, 3H, aromatic), 4.52 (s, 2H, CH_2CO), 4.33 (d, 2H, CH_2N), 3.62 (bd, 1H, CH), 2.84−2.74 (m, 3H, CH_2 + C*H*H), 2.32 (dd, 1H, CH*H*), 1.87−1.75 (m, 4H, 2 CH_2). $C_{22}H_{20}N_4O_6S$; MW: 468; MS 469 $[M + H]^+$.

5-Carbamoylmethyl-4-*oxo*-3,4,5,6,7,8-hexahydro-benzo[4,5]thieno[2,3-*d*]pyrimidine-2-carboxylic Acid (3-*oxo*-3,4-dihydro-2*H*-benzo[1,4]oxazin-6-yl-methyl)amide (2). To a solution of acid **14** (20 mg, 43 μmol), EDCI (16 mg, 71 μmol) and HOAt (6 mg, 43 μmol) in DMF (3 mL) were added NMM (100 μL) and ammonium chloride (3 mg, 51 μmol). The mixture was stirred overnight at room temperature and then concentrated. The remaining residue was suspended in 10% aqueous citric acid and the residue was filtered and dried to afford the title compound (13.7 mg, 69%) as an off-white solid. ^{1}H NMR (DMSO-d_6): δ 12.36 (bs, 1H, NH), 10.68 (s, 1H, NH), 9.63 (t, 1H, NH), 7.14 (s, 1H; N*H*H), 6.89 (m, 3H, aromatic), 6.81 (s, 1H, NH*H*), 4.52 (s, 2H, CH_2O), 4.33 (d, 2H, CH_2NH), 3.60 (bd, 1H, CH), 2.89−2.61 (m, 4H, CH_2CON + CH_2), 2.18−1.68 (m, 4H, 2 CH_2). Anal. ($C_{22}H_{21}N_5O_5S$) C, H, N, S. MW: 467; MS 468 $[M + H]^+$.

Enzyme Assay for Determination of the Inhibition Constants IC_{50}. MMP-8 activity and the selectivity assays were performed using the catalytic domains of recombinant human MMPs (MMP-

Table 3. Statistics of Crystallographic Data and Refinement

	MMP-8:(*S*)-**2** (without AH)	MMP-8:**1** (with AH)	MMP-8:**1** (with AH)
wavelength (Å)	0.8726	0.8726	0.8726
temperature (K)	100	100	100
space group	*P*21 monoclinic	*P*21 monoclinic	*P*21212 orthorhombic
no. of mol in the AU	2	1	2
cell axes (Å)	42.34; 69.38; 52.71	32.29; 68.95; 32.75	68.30; 69.21; 81.23
beta angle (deg)	92.35	105.41	
resolution range (Å)	25.00−2.00 (2.12−2.00)[a]	25.00−1.60 (1.69−1.60)[a]	25.00−2.10 (2.20−2.10)[a]
R_{merge} (%)	12.4 (29.7)[a]	10.3 (30.9)[a]	11.9 (30.9)[a]
multiplicity	3.1 (3.1)[a]	4.1 (3.9)[a]	4.1 (4.0)[a]
I/σ (I)	3.6 (2.2)[a]	5.7 (2.4)[a]	4.0 (2.0)[a]
completeness (%)	99.6 (100)[a]	99.2 (96.1)[a]	96.9 (80.6)[a]
R_{factor} (%)	22.0	21.0	23.8
R_{free} (%)	28.0	24.2	27.0
no. of reflections (work)	19025	16280	20614
no. of reflections (test)	1400	1780	1519
rmsd bond lengths/bond angles	0.006/1.293	0.005/1.439	0.006/1.270
Ramachandran plot favored/ allowed/generously allowed (%)	86.6/12.3/1.1	84.8/13.0/1.4	89.5/9.8/0.7
protein nonhydrogen atoms	2568	1284	2568
solvent molecules	361	216	426
nonhydrogen inhibitors atoms	66	37	74
ions	8	4	8
protein average *B* factors (Å^2)	17.0	8.8	18.8
water ave. *B* factors (Å^2)	35.8	21.9	37.6
inhibitor ave. *B* factors (Å^2)	16.2	13.7	24.8
ions ave. *B* factors (Å^2)	10.8	4.2	13.0

[a] The values in parentheses refer to the outer shell.

1, −2, −3, −7, −9, −12: Biomol, Hamburg, Germany; MMP-8: Calbiochem, Schwalbach, Germany; MMP-13 and MMP-14: Invitek, Berlin, Germany) and the appropriate fluorogenic peptide substrate. MMP-13 activity was tested using the specific MMP-13 substrate MCA-Pro-Cha-Gly-Nva-His-Ala-Dpa-NH_2 (Calbiochem, Schwalbach, Germany). MMP-3 was tested using the NFF-3 substrate MCA-Arg-Pro-Lys-Pro-Val-Glu-Nva-Trp-Arg-Lys(DNP)-NH_2 (Calbiochem, Schwalbach, Germany) and all remaining MMPs were tested using OmniMMP substrate MCA-Pro-Leu-Gly-Leu-Dpa-Ala-Arg-NH_2·AcOH (Biomol, Hamburg, Germany).[51]

The MMP-3 assay was performed in 50 mM MES buffer, pH 6.0, 10 mM $CaCl_2$ and 0.05% Brij-35. All other MMP assays were performed in 50 mM Tris-HCl buffer, pH 7.5, 150 mM NaCl, 5 mM $CaCl_2$, and 0.05% Brij-35. Concentrations of enzymes and substrates were optimized for each assay and varied between 1 and 10 nM enzyme and 4−10 μM substrate. The enzyme activity was measured after 10 min preincubation of the enzyme with varying concentrations of the inhibitor. Each assay was run at least in duplicate and the IC_{50} values were calculated using Life Science Workbench (LSW) Data Analysis Plugin for Microsoft Excel. The data were fitted into the formula $y = V_{max}/(1 + ([I]/IC_{50})$.

Expression and Purification of the Protein. The truncated form M80-G242 of the catalytic domain of MMP-8 has been supplied by Prof. H. Tschesche, University of Bielefeld (Germany). The protocol of expression and purification has been previously described.[52]

Protein Crystallization. Acetohydroxamate (AH) was added to 45 mL of protein solution (MMP-8 2.4 μM, in 5 mM Tris HCl, pH 7.0, 100 mM NaCl and 5 mM $CaCl_2$) to a final concentration of 50 mM. The weak inhibitor AH was added to the protein solution to aid protein stability by preventing autoproteolysis during concentration. However, 15 mL of protein solution have been used for crystallization trials without AH in order to check whether the binding mode of the inhibitors could be perturbed by the presence of AH. The MMP-8 protein with AH was concentrated with Amicon-Ultra 15, dialyzing with the crystallization solution (5 mM $CaCl_2$, 100 mM NaCl, 0.5 mM $ZnCl_2$, 3 mM MES-NaOH, 0.02% NaN_3, pH 6.0) to a final concentration of 5.8 mg/mL. The protein solution was equilibrated with the inhibitor stock solutions (100 mM in DMSO) at 4 °C overnight, so that the inhibitor were 5-fold in excess and the final concentration of DMSO 1.5%. Crystallizations were performed by hanging-drop vapor diffusion at 18 °C. Hanging droplets were made by mixing 1.5−3.0 μL of protein/inhibitor solution with 5 μL of PEG solution (10% (m/v) PEG6000, 0.2 M Mes-NaOH, 0.02% NaN_3, pH 6.0). Droplets were concentrated against a reservoir buffer containing 1.0−2.0 M sodium phosphate, 0.02% NaN_3, pH 6.0. Crystals appeared in 3−4 days.

The inhibitor from the stock solution was added to the protein solution without AH in large excess and complexation was allowed to continue overnight at 4 °C. The complex was then concentrated, dialysing with the crystallization solution, up to 2−3 mg/mL. More than half of the protein has been lost during the concentration, cleaved, and absorbed to the filter. Only 10 drops of crystallization could be made, by mixing 2.5−3 μL of protein solution with 5 μL of PEG solution. The reservoir was made of 1.7−2.0 M sodium phosphate, pH 6.0. Crystals appeared in 3−7 days.

Data Collection and Processing. X-ray data were collected under cryogenic conditions (100 K) at the ID23-2 microfocus beamline of ESRF, Grenoble, using a wavelength of 0.873 Å and a MAR-Mosaic225 CCD detector. The crystals were flash-frozen in the nitrogen stream after transferring them for few seconds into the mother solution containing 35% PEG400. Data were integrated and scaled using the programs MOSFLM and SCALA.[53] The statistics of collection and refinement is given in Table 3.

Structure Solution and Refinement. The orientation and translation of the protein molecules within the crystallographic unit cell was determined using the program AmoRe[54] with the coordinates of MMP-8 (PDB accession code 1I76[55]) as a search model. Using data in the 12−3 Å resolution range an unambiguous solution was obtained for each complex. All the structures were refined with CNS.[56] The R_{free} validation was based on a subset of 7% (10% for the monoclinic form of MMP-8:**1**) of the reflections omitted during the refinement. The inhibitors were fitted manually into the $F_o - F_c$ electron density and unambiguously modeled. After several rounds of refinement water molecules were added.

Acknowledgment. We acknowledge G. Becher, M. Burger, H. Kheil, A. Timmermann, and J. Weik from Alantos Pharmaceuticals AG for the determination of the IC_{50} values and Fulvio Loiodice from Dipartimento Farmaco-Chimico, Università degli Studi di Bari, for the elemental analysis.

Supporting Information Available: C^{α} distances at the S_1' loop region between the uninhibited MMP-8 and the inhibited complexes MMP-8:**1** and MMP-8:(*S*)-**2**, elemental analysis data, and NMR spectra of compounds **1** and **2**. This material is available free of charge via the Internet at http://pubs.acs.org.

References

(1) Sternlicht, M. D.; Werb, Z. How matrix metalloproteinases regulate cell behavior. *Annu. Rev. Cell Dev. Biol.* **2001**, *17*, 463–516.

(2) Shapiro, S. D. Matrix metalloproteinase degradation of extracellular matrix: biological consequences. *Curr. Opin. Cell Biol.* **1998**, *10*, 602–608.

(3) Whittaker, M.; Floyd, C. D.; Brown, P.; Gearing, A. J. Design and therapeutic application of matrix metalloproteinase inhibitors. *Chem. Rev.* **1999**, *99*, 2735–2776.

(4) Overall, C. M.; López-Otin, C. Strategies for MMP inhibition in cancer: innovations for the post-trial era. *Nat. Rev. Cancer* **2002**, *2*, 657–672.

(5) Holleran, W. M.; Galardy, R. E.; Gao, W. N.; Levy, D.; Tang, P. C.; Elias, P. M. Matrix metalloproteinase inhibitors reduce phorbol ester-induced cutaneous inflammation and hyperplasia. *Arch. Dermatol. Res.* **1997**, *289*, 138–144.

(6) Hewson, A. K.; Smith, T.; Leonard, J. P.; Cuzner, M. L. Suppression of experimental allergic encephalomyelitis in the Lewis rat by the matrix metalloproteinase inhibitor Ro31-9790. *Inflamm. Res.* **1995**, *44*, 345–349.

(7) Chandler, S.; Coates, R.; Gearing, A.; Lury, J.; Wells, G.; Bone, E. Matrix metalloproteinases degrade myelin basic protein. *Neurosci. Lett.* **1995**, *201*, 223–226.

(8) Lohmander, L. S.; Hoerrner, L. A.; Lark, M. W. Metalloproteinases, tissue inhibitor, and proteoglycan fragments in knee synovial fluid in human osteoarthritis. *Arthritis Rheum.* **1993**, *36*, 181–189.

(9) Ahrens, D.; Koch, A. E.; Pope, R. M.; Stein-Picarella, M.; Niedbala, M. J. Expression of matrix metalloproteinase 9 (96-kd gelatinase B) in human rheumatoid arthritis. *Arthritis Rheum.* **1996**, *39*, 1576–1587.

(10) Blaser, J.; Triebel, S.; Maasjosthusmann, U.; Romisch, J.; Krahl-Mateblowski, U.; Freudenberg, W.; Fricke, R.; Tschesche, H. Determination of metalloproteinases, plasminogen-activators and their inhibitors in the synovial fluids of patients with rheumatoid arthritis during chemical synoviorthesis. *Clin. Chim. Acta* **1996**, *244*, 17–33.

(11) Ohishi, K.; Fujita, N.; Morinaga, Y.; Tsuruo, T. H-31 human breast cancer cells stimulate type I collagenase production in osteoblast-like cells and induce bone resorption. *Clin. Exp. Metastasis* **1995**, *13*, 287–295.

(12) Witty, J. P.; Foster, S. A.; Stricklin, G. P.; Matrisian, L. M.; Stern, P. H. Parathyroid hormone-induced resorption in fetal rat limb bones is associated with production of the metalloproteinases collagenase and gelatinase B. *J. Bone Miner. Res.* **1996**, *11*, 72–78.

(13) Peress, N.; Perillo, E.; Zucker, S. Localization of tissue inhibitor of matrix metalloproteinases in Alzheimer's disease and normal brain. *J. Neuropathol. Exp. Neurol.* **1995**, *54*, 16–22.

(14) Chang, C.; Werb, Z. The many faces of metalloproteases: cell growth, invasion, angiogenesis and metastasis. *Trends Cell. Biol.* **2001**, *11*, S37−S43.

(15) Coussens, L. M.; Fingleton, B.; Matrisian, L. M. Matrix metalloproteinase inhibitors and cancer: trials and tribulations. *Science* **2002**, *295*, 2387–2392.

(16) Puerta, D. T.; Cohen, S. M. A bioinorganic perspective on matrix metalloproteinase inhibition. *Curr. Top. Med. Chem.* **2004**, *4*, 1551–1573.

(17) Matter, H.; Schudok, M. Recent advances in the design of matrix metalloprotease inhibitors. *Curr. Opin. Drug Discovery Dev.* **2004**, *7*, 513–535.

(18) Fingleton, B. Matrix metalloproteinases as valid clinical targets. *Curr. Pharm. Des.* **2007**, *13*, 333–346.

(19) Skiles, J. W.; Gonnella, N. C.; Jeng, A. Y. The design, structure, and clinical update of small molecular weight matrix metalloproteinase inhibitors. *Curr. Med. Chem.* **2004**, *11*, 2911–2977.

(20) Rao, B. G. Recent developments in the design of specific matrix metalloproteinase inhibitors aided by structural and computational studies. *Curr. Pharm. Des.* **2005**, *11*, 295–322.

(21) Babine, R. E.; Bender, S. L. Molecular recognition of protein−ligand complexes: applications to drug design. *Chem. Rev.* **1997**, *97*, 1359–1472.

(22) Grams, F.; Crimmin, M.; Hinnes, L.; Huxley, P.; Pieper, M.; Tschesche, H.; Bode, W. Structure determination and analysis of human neutrophil collagenase complexed with a hydroxamate inhibitor. *Biochemistry* **1995**, *34*, 14012–14020.

(23) Muri, E. M.; Nieto, M. J.; Sindelar, R. D.; Williamson, J. S. Hydroxamic acids as pharmacological agents. *Curr. Med. Chem.* **2002**, *9*, 1631–1653.

(24) Levin, J. I. The design and synthesis of aryl hydroxamic acid inhibitors of MMPs and TACE. *Curr. Top. Med. Chem.* **2004**, *4*, 1289–1310.

(25) Freskos, J. N.; McDonald, J. J.; Mischke, B. V.; Mullins, P. B.; Shieh, H. S.; Stegeman, R. A.; Stevens, A. M. Synthesis and identification of conformationally constrained selective MMP inhibitors. *Bioorg. Med. Chem. Lett.* **1999**, *9*, 1757–1760.

(26) Tamura, Y.; Watanabe, F.; Nakatani, T.; Yasui, K.; Fuji, M.; Komurasaki, T.; Tsuzuki, H.; Maekawa, R.; Yoshioka, T.; Kawada, K.; Sugita, K.; Ohtani, M. Highly selective and orally active inhibitors of type IV collagenase (MMP-9 and MMP-2): *N*-sulfonylamino acid derivatives. *J. Med. Chem.* **1998**, *41*, 640–649.

(27) Hodgson, J. Remodeling MMPIs. *Biotechnology (N.Y.)* **1995**, *13*, 554–557.

(28) Puerta, D. T.; Lewis, J. A.; Cohen, S. M. New beginnings for matrix metalloproteinase inhibitors: identification of high-affinity zinc-binding groups. *J. Am. Chem. Soc.* **2004**, *126*, 8388–8389.

(29) Puerta, D. T.; Mongan, J.; Tran, B. L.; McCammon, J. A.; Cohen, S. M. Potent, selective pyrone-based inhibitors of stromelysin-1. *J. Am. Chem. Soc.* **2005**, *127*, 14148–14149.

(30) Jacobsen, F. E.; Lewis, J. A.; Cohen, S. M. A new role for old ligands: discerning chelators for zinc metalloproteinases. *J. Am. Chem. Soc.* **2006**, *128*, 3156–3157.

(31) Li, X.; Li, Y.; Xu, W. Design, synthesis, and evaluation of novel galloyl pyrrolidine derivatives as potential antitumor agents. *Bioorg. Med. Chem.* **2006**, *14*, 1287–1293.

(32) Zhang, L.; Zhang, J.; Fang, H.; Wang, Q.; Xu, W. Design, synthesis and preliminary evaluation of new cinnamoyl pyrrolidine derivatives as potent gelatinase inhibitors. *Bioorg. Med. Chem.* **2006**, *14*, 8286–8294.

(33) Campestre, C.; Agamennone, M.; Tortorella, P.; Preziuso, S.; Biasone, A.; Gavuzzo, E.; Pochetti, G.; Mazza, F.; Hiller, O.; Tschesche, H.; Consalvi, V.; Gallina, C. *N*-Hydroxyurea as zinc binding group in matrix metalloproteinase inhibition: mode of binding in a complex with MMP-8. *Bioorg. Med. Chem. Lett.* **2006**, *16*, 20–24.

(34) Mannino, C.; Nievo, M.; Machetti, F.; Papakyriakou, A.; Calderone, V.; Fragai, M.; Guarna, A. Synthesis of bicyclic molecular scaffolds (BTAa): an investigation towards new selective MMP-12 inhibitors. *Bioorg. Med. Chem.* **2006**, *14*, 7392–7403.

(35) Nuti, E.; Tuccinardi, T.; Rossello, A. Matrix metalloproteinase inhibitors: new challenges in the era of post broad-spectrum inhibitors. *Curr. Pharm. Des.* **2007**, *13*, 2087–2100.

(36) Pirard, P. Insight into the structural determinants for selective inhibition of metalloproteinases. *Drug Discovery Today* **2007**, *12*, 640–646.

(37) Georgiadis, D.; Yiotakis, A. Specific targeting of metzincin family members with small-molecule inhibitors: progress toward a multifarious challenge. *Bioorg. Med. Chem.* **2008**, *16*, 8781–8794.

(38) Chen, J. M.; Nelson, F. C.; Levin, J. I.; Mobilio, D.; Moy, F. J.; Nilakantan, R.; Zask, A.; Powers, R. Structure-based design of a novel, potent, and selective inhibitor for MMP-13 utilizing NMR spectroscopy and computer-aided molecular design. *J. Am. Chem. Soc.* **2000**, *122*, 9648–9654.

(39) Engel, C. K.; Pirard, B.; Schimanski, S.; Kirsch, R.; Habermann, J.; Klingler, O.; Schlotte, V.; Weithmann, K. U.; Wendt, K. U. Structural basis for the highly selective inhibition of MMP-13. *Chem. Biol.* **2005**, *12*, 181–189.

(40) Morales, R.; Perrier, S.; Florent, J. M.; Beltra, J.; Dufour, S.; De Mendez, I.; Manceau, P.; Tertre, A.; Moreau, F.; Compere, D.; Dublanchet, A. C.; O'Gara, M. Crystal structures of novel non-peptidic, non-zinc chelating inhibitors bound to MMP-12. *J. Mol. Biol.* **2004**, *341*, 1063–1076.

(41) Johnson, A. R.; Pavlovsky, A. G.; Ortwine, D. F.; Prior, F.; Man, C. F.; Bornemeier, D. A.; Banotai, C. A.; Mueller, W. T.; McConnell, P.; Yan, C.; Baragi, V.; Lesch, C.; Roark, W. H.; Wilson, M.; Datta, K.; Guzman, R.; Han, H. K.; Dyer, R. D. Discovery and characterization of a novel inhibitor of matrix metalloprotease-13 that reduces cartilage damage in vivo without joint fibroplasia side effects. *J. Biol. Chem.* **2007**, *282*, 27781–27791.

(42) Li, J. J.; Nahra, J.; Johnson, A. R.; Bunker, A.; O'Brien, P.; Yue, W. S.; Ortwine, D. F.; Man, C. F.; Baragi, V.; Kilgore, K.; Dyer, R. D.; Han, H. K. Quinazolinones and pyrido[3,4-*d*]pyrimidin-4-ones as orally active and specific matrix metalloproteinase-13 inhibitors for the treatment of osteoarthritis. *J. Med. Chem.* **2008**, *51*, 835–841.

(43) Overall, C. M.; Kleifeld, O. Tumour microenvironment−opinion: validating matrix metalloproteinases as drug targets and antitargets for cancer therapy. *Nat. Rev. Cancer* **2006**, *6*, 227–239.

(44) Van Lint, P.; Wielockx, B.; Puimège, L.; Noël, A.; López-Otin, C.; Libert, C. Resistance of collagenase-2 (matrix metalloproteinase-8)-deficient mice to TNF-induced lethal hepatitis. *J. Immunol.* **2005**, *175*, 7642–7649.

(45) Folgueras, A. R.; Fueyo, A.; Garcia-Suárez, O.; Cox, J.; Astudillo, A.; Tortorella, P.; Campestre, C.; Gutiérrez-Fernández, A.; Fanjul-Fernández, M.; Pennington, C. J.; Edwards, D. R.; Overall, C. M.; López-Otin, C. Collagenase-2 deficiency or inhibition impair experi-

mental autoimmune encephalomyelitis in mice. *J. Biol. Chem.* **2008**, *283*, 9465–9474.
(46) Van Lint, P.; Libert, C. Matrix metalloproteinase-8: cleavage can be decisive. *Cytokine Growth Factor Rev.* **2006**, *17*, 217–223.
(47) Gege, C.; Cevrier, C.; Schneider, M.; Bluhm, H.; Hochgürtel, M.; Deng, H.; Gallagher, B.; Sucholeiki, I.; Taveras, A. G. Heterotricyclic metalloprotease inhibitors. PCT Int. Appl. WO2008063667, 2008.
(48) Bertini, I.; Calderone, V.; Fragai, M.; Luchinat, C.; Maletta, M.; Yeo, K. J. Snapshots of the reaction mechanism of matrix metalloproteinases. *Angew. Chem., Int. Ed.* **2006**, *45*, 7952–7955.
(49) Teague, S. J. Implications of protein flexibility for drug discovery. *Nat. Rev. Drug Discovery* **2003**, *2*, 527–541.
(50) Steeneck, C.; Gege, C.; Richter, F.; Hochgürtel, M.; Feuerstein, T.; Bluhm, H.; Sucholeiki, I.; Boer, J.; Wu, X.; Schneider, M.; Nolte, B.; Gallagher, B.; van Veldhuizen, J.; Deng, H.; Essers, M.; Kroth, H.; Kiely, A.; Powers, T.; Taveras, A. G. Pyrimidine or triazine fused bicyclic metalloprotease inhibitors. PCT Int. Appl. WO2006128184, 2006.
(51) Knight, C. G.; Willenbrock, F.; Murphy, G. A novel coumarin-labelled peptide for sensitive continuous assays of the matrix metalloproteinases. *FEBS Lett.* **1992**, *296*, 263–266.
(52) Schnierer, S.; Kleine, T.; Gote, T.; Hillemann, A.; Knauper, V.; Tschesche, H. The recombinant catalytic domain of human neutrophil collagenase lacks type I collagen substrate specificity. *Biochem. Biophys. Res. Commun.* **1993**, *191*, 319–326.
(53) Leslie, A. G. W. *Joint CCP4 and ESF-EACMB Newsletters on Protein Crystallography*; SERC Daresbury Laboratory: Warrington, UK, 1992; Vol. 26.
(54) Navaza, J. AMoRe: an automated package for molecular replacement. *Acta Crystallogr., Sect. A: Found. Crystallogr.* **1994**, *50*, 157–163.
(55) Gavuzzo, E.; Pochetti, G.; Mazza, F.; Gallina, C.; Gorini, B.; D'Alessio, S.; Pieper, M.; Tschesche, H.; Tucker, P. A. Two crystal structures of human neutrophil collagenase, one complexed with a primed- and the other with an unprimed-side inhibitor: implications for drug design. *J. Med. Chem.* **2000**, *43*, 3377–3385.
(56) Brunger, A. T.; Adams, P. D.; Clore, G. M.; DeLano, W. L.; Gros, P.; Grosse-Kunstleve, R. W.; Jiang, J. S.; Kuszewski, J.; Nilges, M.; Pannu, N. S.; Read, R. J.; Rice, L. M.; Simonson, T.; Warren, G. L. Crystallography & NMR system: a new software suite for macromolecular structure determination. *Acta Crystallogr., Sect. D: Biol. Crystallogr.* **1998**, *54* (Pt 5), 905–921.

JM801166J